On localization of Dirac fermions by disorder

Medvedyeva, M.V.

Citation

Medvedyeva, M. V. (2011, May 3). *On localization of Dirac fermions by disorder. Casimir PhD Series*. Retrieved from https://hdl.handle.net/1887/17606

Chapter 4

Majorana bound states without vortices in topological superconductors with electrostatic defects

4.1 Introduction

Two-dimensional superconductors with spin-polarized-triplet, p-wave pairing symmetry have the unusual property that vortices in the order parameter can bind a nondegenerate state with zero excitation energy [64, 124, 97, 53]. Such a midgap state is called a Majorana bound state, because the corresponding quasiparticle excitation is a Majorana fermion — equal to its own antiparticle. A pair of spatially separated Majorana bound states encodes a qubit, in a way which is protected from any local source of decoherence [62]. Since such a qubit might form the building block of a topological quantum computer [84], there is an intensive search [57, 116, 105, 106, 68, 4] for two-dimensional superconductors with the required combination of broken time-reversal and spin-rotation symmetries (symmetry class D [6]).

The generic Bogoliubov-De Gennes Hamiltonian H of a chiral p-wave superconductor is only constrained by particle-hole symmetry, $\sigma_x H^* \sigma_x = -H$. At low excitation energies E (to second order in mo-

mentum $p = -i\hbar \partial/\partial r$) it has the form

$$H = \Delta\big(p_x\sigma_x + p_y\sigma_y\big) + \big(U(r) + p^2/2m\big)\sigma_z, \qquad (4.1)$$

for a uniform (vortex-free) pair potential Δ. The electrostatic potential U (measured relative to the Fermi energy) opens up a band gap in the excitation spectrum. At $U = 0$ the superconductor has a topological phase transition (known as the thermal quantum Hall effect) between two localized phases, one with and one without chiral edge states [123, 109, 121, 122].
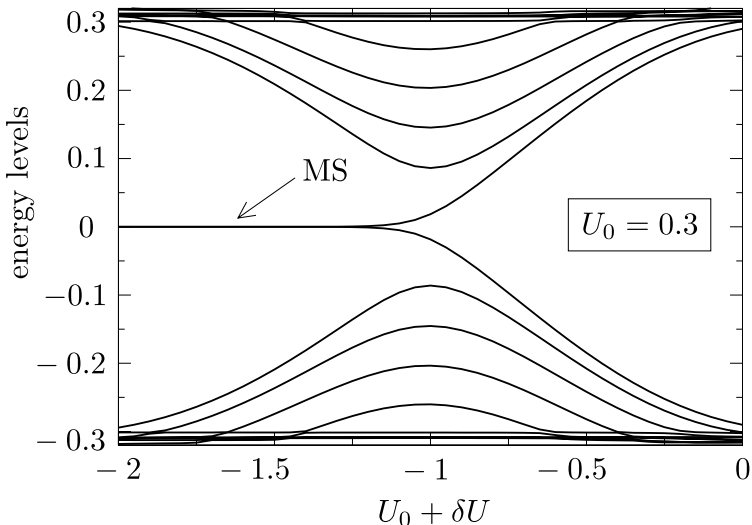

Figure 4.1. Emergence of a pair of zero-energy MS states as the defect potential $U_0 + \delta U$ is made more and more negative, at fixed positive background potential $U_0 = 0.3$. (All energies are in units of $\gamma \equiv \hbar\Delta/a$.) The energy levels are the eigenvalues of the Hamiltonian (4.1) on a square lattice (dimension $100\,a \times 100\,a$, $\beta \equiv \hbar^2/2ma^2 = 0.4\,\gamma$, periodic boundary conditions). The line defect has length $50\,a$. The dense spectrum at top and bottom consists of bulk states.

4.2   Majorana-Shockley bound states in lattice Hamiltonians

Our key observation is that the Hamiltonian (4.1) on a lattice has Majorana bound states at the two end points of a linear electrostatic defect

(consisting of a perturbation of U on a string of lattice sites). The mechanism for the production of these bound states goes back to Shockley [110]: The band gap closes and then reopens upon formation of the defect, and as it reopens a pair of states splits off from the band edges to form localized states at the end points of the defect (see Fig. 4.1). Such Shockley states appear in systems as varied as metals and narrow-band semiconductors [31], carbon nanotubes [107], and photonic crystals [77]. In these systems they are unprotected and can be pushed out of the band gap by local perturbations. In a superconductor, in contrast, particle-hole symmetry requires the spectrum to be $\pm E$ symmetric, so an isolated bound state is constrained to lie at $E = 0$ and cannot be removed by any local perturbation.

We propose the name Majorana-Shockley (MS) bound state for this special type of topologically protected Shockley states. Similar states have been studied in the context of lattice gauge theory by Creutz and Horváth [30, 29], for an altogether different purpose (as a way to restore chiral symmetry in the Wilson fermion model of QCD [126]).

Consider a square lattice (lattice constant a), at uniform potential U_0. The Hamiltonian (4.1) on the lattice has dispersion relation

$$E^2 = [U_0 + 2\beta(2 - \cos ak_x - \cos ak_y)]^2 + \gamma^2 \sin^2 ak_x + \gamma^2 \sin^2 ak_y. \quad (4.2)$$

(We have defined the energy scales $\beta = \hbar^2/2ma^2$, $\gamma = \hbar\Delta/a$.) The spectrum becomes gapless for $U_0 = 0$, -4β, and -8β, signaling a topological phase transition [95]. The number of edge states is zero for $U_0 > 0$ and $U_0 < -8\beta$, while it is unity otherwise (with a reversal of the direction of propagation at $U_0 = -4\beta$). The topologically nontrivial regime is therefore reached for U_0 negative, but larger than -8β.

We now introduce the electrostatic line defect by changing the potential to $U_0 + \delta U$ on the N lattice points at $\boldsymbol{r} = (na, 0)$, $n = 1, 2, \ldots N$. In Figs. 4.1 and 4.2 we show the closing and reopening of the band gap as the defect is introduced, accompanied by the emergence of a pair of states at zero energy. The eigenstates for which the gap closes and reopens have wave vector k_x parallel to the line defect equal to either 0 or $\pm\pi/a$ (in the limit $N \to \infty$ when k_x is a good quantum number).

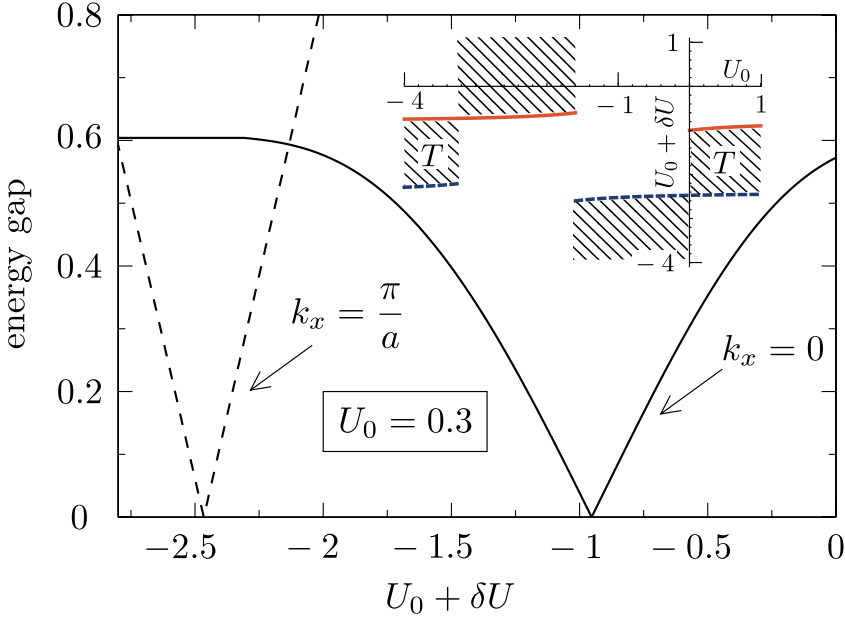We have calculated that the gap closing at $k_x = 0$ happens at a critical

Figure 4.2. Main plot: Closing and reopening of the excitation gap at $U_0 = 0.3$, $\beta = 0.4$ (in units of γ), for states with $k_x = 0$ (black solid curve) and $k_x = \pi/a$ (black dashed curve). The MS states exist for defect potentials in between two gap-closings, indicated as a function of U_0 by the shaded regions in the inset. (The red solid and blue dashed curves show, respectively $U_0 + \delta U_0$ and $U_0 + \delta U_\pi$. The label T indicates the topologically trivial phase.)

potential $\delta U = \delta U_0$ given by (derived in Section 4.A)

$$\delta U_0 = \begin{cases} -\sqrt{U_0(U_0 + 4\beta) + \gamma^2} & \text{for } U_0 > 0, \\ \sqrt{U_0(U_0 + 4\beta) + \gamma^2} & \text{for } U_0 < -4\beta, \\ \text{no finite value otherwise.} \end{cases} \qquad (4.3)$$

The critical potential δU_π for closing of the gap at $k_x = \pm\pi/a$ is obtained from Eq. (4.3) by the replacement of U_0 with $U_0 + 4\beta$. The MS states appear for defect potentials $U_0 + \delta U$ in between two subsequent gap closings, as indicated in the inset of Fig. 4.2.

We conclude that MS states exist for any value of U_0. In contrast, Majorana bound states in vortices exist only in the topologically non-trivial regime [97, 47]. The index theorem [101] for the production of zero-energy modes by the vortex mechanism, which requires the topo-
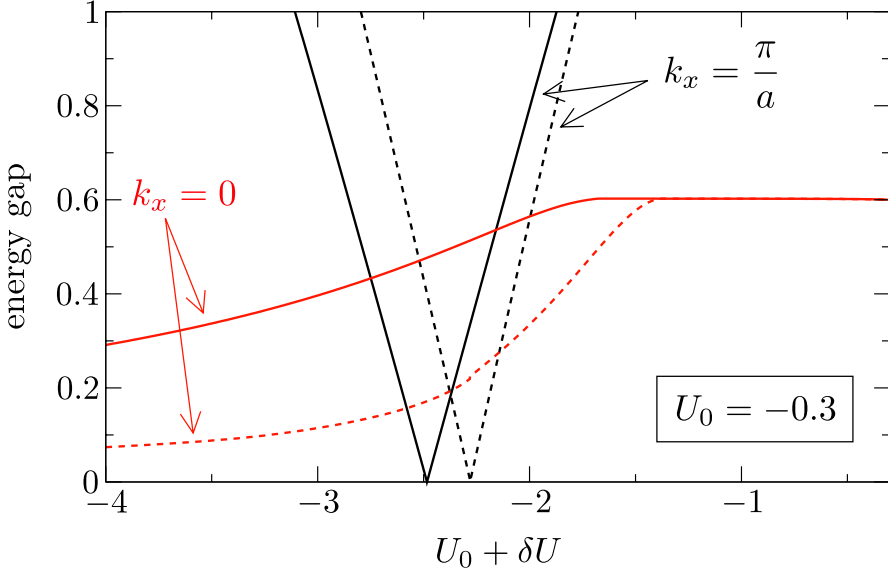
Figure 4.3. Closing and reopening of the excitation gap at $U_0 = -0.3$, $\beta = 0.4$ (in units of γ), for states with $k_x = 0$ (red curves) and $k_x = \pi/a$ (black curves). The results were obtained from numerical calculations using a constant isotropic pair potential Δ (solid lines) as in Fig. 4.2 as well as a spatially dependent, anisotropic pair potential $(\Delta_x(r), \Delta_y(r))$ determined self-consistently from the gap equation (dashed lines), Sec. 4.B.

logically nontrivial phase, is therefore not applicable to the Shockley mechanism.

Our reasoning so far has relied on the assumption of a constant pair potential Δ, unperturbed by the defect. In order to demonstrate the robustness of the Majorana-Shockley mechanism, we have performed numerical calculations that determine the pair potential self-consistently by means of the gap equation [44], Sec. 4.B. In Fig. 4.3 we show a comparison of the closing and reopening of the band gap as obtained from calculations with and without self-consistency, in the relevant weak pairing regime ($U_0 < 0$). The self-consistency does not change the qualitative behavior. In particular, the gap only closes at $k_x = \pi/a$ for the parameters chosen (c.f. inset in Fig. 4.2) and the self-consistent determination of Δ only shifts the critical potential δU slightly.

In Fig. 4.4 we demonstrate that the MS states are localized at the end points of the line defect. The exponentially small, but nonzero overlap
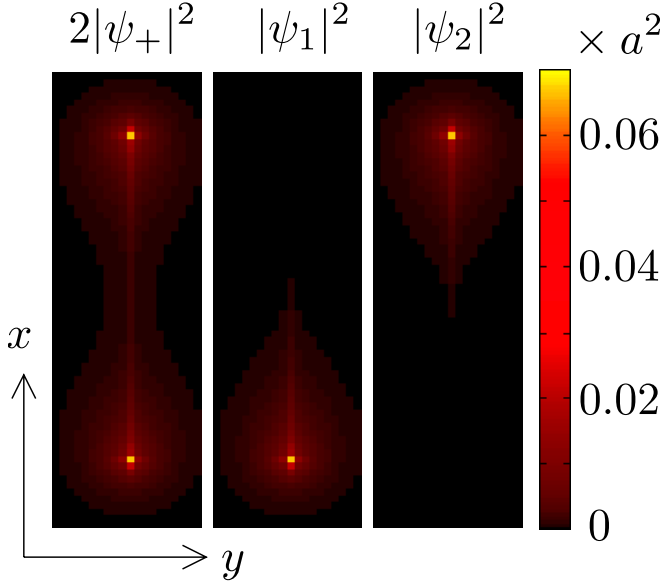
Figure 4.4. Probability density of the paired (ψ_+) and unpaired (ψ_1, ψ_2) Majorana bound states at the end points of a line defect of length $50\,a$, calculated for $U_0 = 0.1\,\gamma$, $U_0 + \delta U = -1.3\,\gamma$, $\beta = 0.4\,\gamma$.

of the pair of states displaces their energy from 0 to $\pm E$ (with corresponding eigenstates $\psi_- = \sigma_x \psi_+^*$ related by particle-hole symmetry). The unpaired Majorana bound states ψ_1 and ψ_2 are given by the linear combinations

$$\psi_1 = \tfrac{1}{2}(1-i)\psi_+ + \tfrac{1}{2}(1+i)\psi_-, \tag{4.4a}$$

$$\psi_2 = \tfrac{1}{2}(1+i)\psi_+ + \tfrac{1}{2}(1-i)\psi_-, \tag{4.4b}$$

shown also in Fig. 4.4. These states are particle-hole symmetric, $\psi_{1,2} = \sigma_x \psi_{1,2}^*$, so the quasiparticle in such a state is indeed equal to its own antiparticle (hence, it is a Majorana fermion).

If the line defect has a width W which extends over several lattice sites, multiple gap closings and reopenings appear at $k_x = 0$ upon increasing the defect potential $U_0 + \delta U \equiv -(\hbar k_F)^2/2m$ to more and more negative values at fixed positive background potential U_0. In the continuum limit $W/a \to \infty$, the gap closes when $qW = n\pi + \nu$, $n = 0, 1, 2, \ldots$ (Sec. 4.C), with $q = [k_F^2 - (m\Delta)^2]^{1/2}$ the real part of the transverse wave vector and $\nu \in (0, \pi)$ a phase shift that depends weakly on the potential.
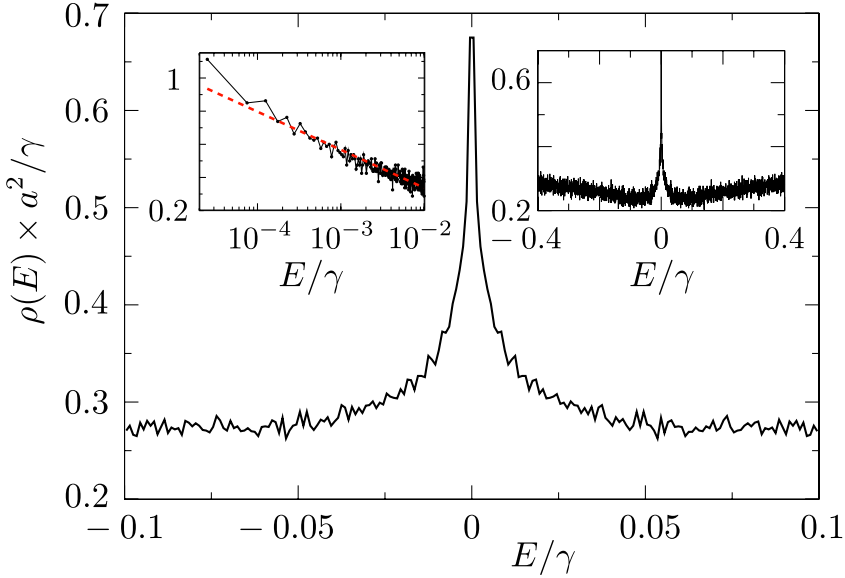
Figure 4.5. Average density of states for a potential that fluctuates randomly from site to site ($\bar{U} = 0.01\,\gamma$, $\Delta U = 2\,\gamma$, $\beta = 0.2\,\gamma$). The lattice has size $400\,a \times 400\,a$. The right inset shows the same data as in the main plot, over a larger energy range. The left inset has a logarithmic energy scale, to show the dependence $\rho \propto \ln|E|$ expected for a thermal metal (red dashed line).

(Similar oscillatory coupling energies of zero-modes have been found in Refs. [26, 73].) The MS states at the two ends of the line defect alternatingly appear and disappear at each subsequent gap closing.

4.3 Electrostatic disorder in *p*-wave superconductors

So far we constructed MS states for a linear electrostatic defect. More generally, we expect a randomly varying electrostatic potential to create a random arrangement of MS states. To test this, we pick $U(\mathbf{r})$ at each lattice point uniformly from the interval $(\bar{U} - \Delta U, \bar{U} + \Delta U)$ and calculate the average density of states $\rho(E)$. The result in Fig. 4.5 shows the expected peak at $E = 0$. This peak is characteristic of a thermal metal, studied previously in models where the Majorana bound states are due to vortices [17, 23, 80]. The theory of a thermal metal [109] predicts a logarithmic profile, $\rho(E) \propto \ln|E|$, for the peak in the density of states,

which is consistent with our data.

Without Majorana bound states, the chiral p-wave superconductor would be in the thermal insulator phase, with an exponentially small thermal conductivity at any nonzero $\bar{U}$ [97, 17, 98, 12]. Our findings imply that electrostatic disorder can convert the thermal insulator into a thermal metal, thereby destroying the thermal quantum Hall effect. Numerical results for this insulator-metal transition are shown in chapter 2.

4.4   Continuum limit for electrostatic defects

These results are all for a specific model of a chiral p-wave superconductor. We will now argue that our findings are generic for symmetry class D (along the lines of a similar analysis of solitons in a polymer chain [54]). Let p be the momentum along the line defect and α a parameter that controls the strength of the defect. Assume that the gap closes at $\alpha = \alpha_0$ and at $p = 0$. (Because of particle-hole symmetry the gap can only close at $p = 0$ or $p = \pm\hbar\pi/a$ and these two cases are equivalent.) For α near α_0 and p near 0 the Hamiltonian in the basis of left-movers and right-movers has the generic form

$$H(\alpha) = \begin{pmatrix} (v_0 + v_1)p & -i(\alpha - \alpha_0) \\ i(\alpha - \alpha_0) & -(v_0 - v_1)p \end{pmatrix}, \qquad (4.5)$$

with velocities $0 < v_1 < v_0$. No other terms to first order in $p = -i\hbar\partial/\partial x$ and $\alpha - \alpha_0$ are allowed by particle-hole symmetry, $H(\alpha) = -H^*(\alpha)$.

The line defect is initially formed by letting α depend on x on a scale much larger than the lattice constant. We set one end of the defect at $x = 0$ and increase α from $\alpha(-\infty) < \alpha_0$ to $\alpha(+\infty) > \alpha_0$. Integration of $H[\alpha(x)]\psi(x) = 0$ then gives the wave function of a zero-energy state bound to this end point,

$$\psi(x) = \begin{pmatrix} \sqrt{v_0/v_1 - 1} \\ \sqrt{v_0/v_1 + 1} \end{pmatrix} \exp\left(-\int_0^x \frac{\alpha(x') - \alpha_0}{\sqrt{v_0^2 - v_1^2}} \, dx' \right). \qquad (4.6)$$

This is one of the two MS states, the second being at the other end of the line defect. We may now relax the assumption of a slowly varying $\alpha(x)$, since a pair of uncoupled zero-energy states cannot disappear without violating particle-hole symmetry.

4.5   Outlook

We have identified a purely electrostatic mechanism for the creation of Majorana bound states in chiral *p*-wave superconductors. The zero-energy (mid-gap) states appear in much the same way as Shockley states in non-superconducting materials, but now protected from any local perturbation by particle-hole symmetry. An experimentally relevant consequence of our findings is that the thermal quantum Hall effect is destroyed by electrostatic disorder (in marked contrast to the electrical quantum Hall effect). A recent proposal to realize Wilson fermions in optical lattices [16] also opens the possibility to observe Majorana-Shockley states using cold atoms.

Our analysis is based on a generic model of a two-dimensional class-*D* superconductor (broken time-reversal and spin-rotation symmetry). An interesting direction for future research is to explore whether Majorana-Shockley bound states exist as well in the other symmetry classes [6]. Since an electrostatic defect preserves time-reversal symmetry, we expect the Majorana-Shockley mechanism to be effective also in class *DIII* (when only spin-rotation symmetry is broken). That class includes proximity-induced *s*-wave superconductivity at the surface of a topological insulator [42] and other experimentally relevant topological superconductors [96, 103, 43].

It would also be interesting to investigate the braiding of two electrostatic defect lines, in order to see whether one obtains the same non-Abelian statistics as for the braiding of vortices [53].

Appendix 4.A   Line defect in lattice fermion models

We calculate the closing and reopening of the excitation gap upon introduction of a line defect in a lattice fermion model with particle-hole symmetry. First we treat the Wilson fermion model [126] considered in the main text, and introduced in the context of topological insulators in Refs. [15, 41]. Then, in order to demonstrate the generic nature of the results, we consider an alternative lattice model, the staggered fermion (or Kogut-Susskind) model [63, 113, 14], introduced in the context of graphene in Refs. [119, 79].

4.A.1 Wilson fermions

The Wilson fermion model has Hamiltonian

$$H = \sum_n c_n^\dagger \mathcal{E}_n c_n - \sum_{n,m \text{ (nearest neighb.)}} c_n^\dagger \mathcal{T}_{nm} c_m. \tag{4.7}$$

Each site n on a two-dimensional square lattice (lattice constant a) has electron and hole states $|e\rangle$ and $|h\rangle$. Fermion annihilation operators for these two states are collected in a vector $c_n = (c_{n,e}, c_{n,h})$. States on the same site are coupled by the 2×2 potential matrix $\mathcal{E}_n$ and states on adjacent sites by the 2×2 hopping matrix $\mathcal{T}_{nm}$, defined by [15, 41]

$$\mathcal{E}_n = \begin{pmatrix} U_n & 0 \\ 0 & -U_n \end{pmatrix}, \quad \mathcal{T}_{nm} = \begin{pmatrix} \beta & \gamma e^{i\theta_{nm}} \\ \gamma e^{-i\theta_{mn}} & -\beta \end{pmatrix}. \tag{4.8}$$

Here U_n is the electrostatic potential on site n and $\theta_{nm} \in [0, \pi]$ is the angle between the vector $\boldsymbol{r}_n - \boldsymbol{r}_m$ and the positive y-axis (so $\theta_{mn} = \pi - \theta_{nm}$). In the continuum limit $a \to 0$, the tight-binding Hamiltonian (4.7) is equivalent to the chiral p-wave Hamiltonian (4.1), with $\beta = \hbar^2/2ma^2$ and $\gamma = \hbar\Delta/a$.

It is convenient to transform from position to momentum representation. For that purpose we take periodic boundary conditions in the y-direction, so that the transverse wavevector (in units of $1/a$) has the discrete values $k_l = 2\pi l/N$, $l = -(N-1)/2, \ldots, -1, 0, 1, \ldots, (N-1)/2$ (for an odd number N of sites in the y-direction). The Fourier transformation from position to momentum representation is carried out by the unitary matrix with elements $[\mathcal{F}]_{nl} = N^{-1/2} e^{ink_l}$. We take an infinitely long system in the x-direction, so the longitudinal wavevector k varies continuously in the interval $(-\pi, \pi]$.

For a uniform potential, $U_n \equiv U_0$ for all n, the Fourier transformed Hamiltonian $H_0(k)$ has matrix elements

$$[H_0(k)]_{ll'} = \delta_{ll'} \mathcal{E}_l(k), \tag{4.9}$$

$$\mathcal{E}_l(k) = U_0 \sigma_z + 2\beta \sigma_z (2 - \cos k - \cos k_l) + \gamma(\sigma_x \sin k + \sigma_y \sin k_l). \tag{4.10}$$

The corresponding dispersion relation is

$$\begin{aligned} E(k, k_l)^2 &= [U_0 + 2\beta(2 - \cos k - \cos k_l)]^2 \\ &\quad + \gamma^2(\sin^2 k + \sin^2 k_l), \end{aligned} \tag{4.11}$$

cf. Eq. (4.2).

A line defect at row n_0 (parallel to the x-axis) adds to H_0 the perturbation

$$[\delta H]_{ll'} = N^{-1}e^{in_0(k_{l'}-k_l)}\delta U\sigma_z.$$ (4.12)

The determinantal equation $\text{Det}\,(H_0 + \delta H - E) = 0$ for eigenenergy E reads

$$\text{Det}\,(1 + \mathcal{F}_0^\dagger \delta U\sigma_z \mathcal{F}_0(H_0 - E)^{-1}) = 0,$$ (4.13)

in terms of an $1 \times N$ matrix $\mathcal{F}_0$ with elements $[\mathcal{F}_0]_{1l} = N^{-1/2}e^{in_0 k_l}$. Sylvester's theorem, $\text{Det}(1 + AB) = \text{Det}(1 + BA)$, allows us to rewrite the determinant in the form

$$\text{Det}\,(1 + \delta U\sigma_z \mathcal{F}_0(H_0 - E)^{-1}\mathcal{F}_0^\dagger) = 0,$$ (4.14)

which reduces to

$$0 = \text{Det}\,\left(1 + \delta U\sigma_z \frac{1}{N}\sum_l \frac{1}{\mathcal{E}_l(k) - E}\right)$$

$$= \text{Det}\,\left(1 + \delta U\sigma_z \frac{1}{N}\sum_l \frac{\mathcal{E}_l(k) + E}{E(k,k_l)^2 - E^2}\right).$$ (4.15)

A zero-mode is a pair of states (one left-mover and one right-mover) at energy $E = 0$. This can only occur at $k = 0$ or $k = \pi$ (because for any eigenenergy E at k there must also be an eigenenergy $-E$ at $-k$). From Eqs. (4.10) and (4.15) we obtain the condition for such a zero-mode,

$$\frac{1}{N}\sum_l \frac{U_0 + 2\beta(1 + \delta - \cos k_l)}{[U_0 + 2\beta(1 + \delta - \cos k_l)]^2 + \gamma^2 \sin^2 k_l} = -\frac{1}{\delta U},$$ (4.16)

where $\delta = 0$ if $k = 0$ and $\delta = 2$ if $k = \pi$. In the limit $N \to \infty$ we may replace the sum by an integral, $N^{-1}\sum_l \to (2\pi)^{-1}\int_{-\pi}^{\pi} dk_l$, which can be evaluated by contour integration. The resulting critical value of δU is given in the main text [Eq. (4.3) and following].

4.A.2   Staggered fermions

The staggered fermion model is a discretization of the Hamiltonian (4.1) without the p^2 term. It is formulated in Refs. [113, 14, 119] in terms of the transfer matrix $\mathcal{M}_m$, which relates the transverse wave functions

$\Psi_{m+1} = \mathcal{M}_m \Psi_m$ at columns m and $m+1$ (parallel to the y-axis). For a line defect along the x-axis, the transfer matrix is m-independent, so we can omit the column number m.

The transfer matrix (at energy E) has the form

$$\mathcal{M} = \frac{1-iX}{1+iX}, \tag{4.17}$$

$$X = (\gamma \mathcal{J})^{-1}(\gamma \sigma_z \mathcal{K} + \tfrac{1}{2}E\sigma_x \mathcal{J} - \tfrac{1}{2}i\sigma_y \mathcal{U}). \tag{4.18}$$

In reference to Eq. (4.1), the parameter $\gamma = \hbar \Delta / a$ for lattice constant a. The $N \times N$ matrices $\mathcal{J}$ and $\mathcal{K}$ have nonzero elements

$$\mathcal{J}_{n,n} = 1, \quad \mathcal{J}_{n,n+1} = \mathcal{J}_{n,n-1} = \tfrac{1}{2}, \tag{4.19}$$

$$\mathcal{K}_{n,n+1} = \tfrac{1}{2}, \quad \mathcal{K}_{n,n-1} = -\tfrac{1}{2}, \tag{4.20}$$

while the potential matrix $\mathcal{U}$ (for a line defect at row n_0) is given by

$$\mathcal{U}_{nn'} = U_0 \mathcal{J}_{nn'} + \tfrac{1}{2}\delta U(\delta_{n,n'}\delta_{n,n_0} + \delta_{n,n'}\delta_{n,n_0+1}$$
$$+ \delta_{n+1,n'}\delta_{n,n_0} + \delta_{n,n'+1}\delta_{n',n_0}). \tag{4.21}$$

In momentum representation, the matrix X has elements

$$X_{ll'} = \mathcal{A}_l \delta_{ll'} - i(\delta U/2\gamma)\sigma_y \frac{v_l^* v_{l'}}{4\cos^2(k_l/2)}, \tag{4.22}$$

where we have defined

$$\mathcal{A}_l = i\sigma_z \tan(k_l/2) + (E/2\gamma)\sigma_x - i(U_0/2\gamma)\sigma_y, \tag{4.23}$$

$$v_l = N^{-1/2}e^{in_0 k_l}(1 + e^{ik_l}). \tag{4.24}$$

The dispersion relation of the staggered fermions is $\tan^2(k/2) = A(k,k_l)^2$, with

$$A(k,k_l)^2 = (E/2\gamma)^2 - \tan^2(k_l/2) - (U_0/2\gamma)^2. \tag{4.25}$$

An eigenstate at energy E and longitudinal wavevector k is an eigenstate of X with eigenvalue $-\tan(k/2)$. The determinantal equation $\text{Det}[X + \tan(k/2)] = 0$ can again be simplified using Sylvester's theorem. The result, analogous to Eq. (4.15), is

$$0 = \text{Det}\left(1 - \frac{\delta U}{2\gamma}i\sigma_y \frac{1}{N}\sum_l \frac{1}{\mathcal{A}_l + \tan(k/2)}\right)$$

$$= \text{Det}\left(1 - \frac{\delta U}{2\gamma}i\sigma_y \frac{1}{N}\sum_l \frac{\mathcal{A}_l - \tan(k/2)}{A(k,k_l)^2 - \tan^2(k/2)}\right). \tag{4.26}$$
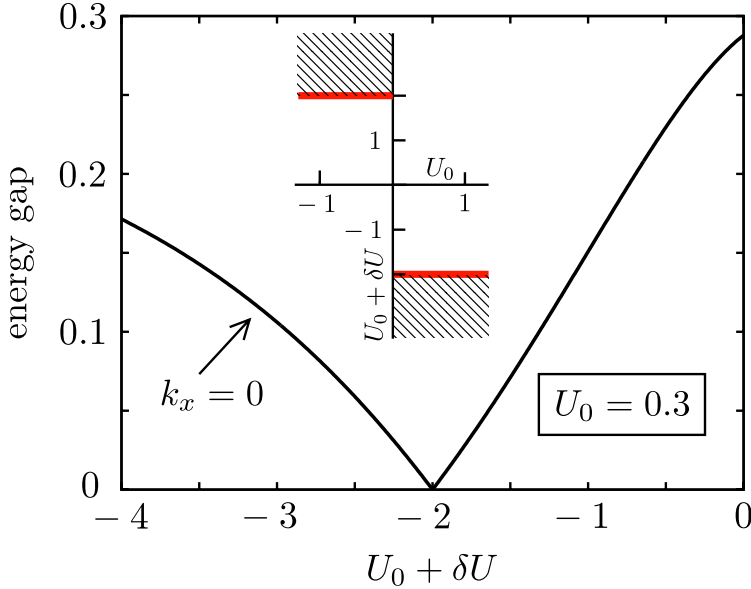
Figure 4.6. Main plot: Closing and reopening of the excitation gap in the staggered fermion model. The MS states exist for defect potentials in the shaded regions in the inset. (All energies are in units of γ.)

Because of the pole in the dispersion relation at $k = \pi$, the zero-mode now exists only at $k = 0$. The condition for this zero-mode, analogous to Eq. (4.16), is

$$\frac{1}{N} \sum_l \frac{U_0/2\gamma}{(U_0/2\gamma)^2 + \tan^2(k_l/2)} = -\frac{2\gamma}{\delta U}, \qquad (4.27)$$

For $N \to \infty$ we may again transform the sum into an integral, and thus obtain the critical potential

$$\delta U = \begin{cases} -U_0 - 2\gamma & \text{if } U_0 > 0, \\ -U_0 + 2\gamma & \text{if } U_0 < 0. \end{cases} \qquad (4.28)$$

Upon varying the potential $U_0 + \delta U$ of the line defect, at fixed bulk potential U_0, the closing and reopening of the gap thus happens at $U_0 + \delta U = -2\gamma \, \text{sign}(U_0)$ (see Fig. 4.6). The inset shows the region in parameter space where the Majorana-Shockley states exist in the staggered fermion model. This phase diagram is much simpler than the corresponding phase diagram for Wilson fermions (Fig. 4.2, inset), because

of the absence of the extra parameter β (which quantifies the strength of the p^2 term in the Wilson fermion model).

Appendix 4.B Self-consistent determination of the pair potential

In order to determine the pair potential self-consistently in a spatially non-homogeneous situation, it is necessary to allow for a position-dependent, anisotropic pair potential $\Delta(r) = (\Delta_x(r), \Delta_y(r))$. The Hamiltonian then reads [44]

$$
\begin{aligned}
H = {}& \tfrac{1}{2} \left\{ \Delta_x(r), p_x \right\} \sigma_x + \tfrac{1}{2} \left\{ \Delta_y(r), p_y \right\} \sigma_y \\
& + \left(U(r) + p^2/2m \right) \sigma_z,
\end{aligned}
\tag{4.29}
$$

where $\{\cdot, \cdot\}$ denotes the anticommutator. In the discretization of this Hamiltonian on a square lattice, the spatial dependence of $\Delta(r)$ is taken into account in the hopping between neighbors as an average value of $\Delta(r)$ on the two lattice points.

When the pair potential is homogeneous, the lattice Hamiltonian has the spectrum

$$
\begin{aligned}
E^2 = {}& [U_0 + 2\beta(2 - \cos ak_x - \cos ak_y)]^2 \\
& + \gamma_x^2 \sin^2 ak_x + \gamma_y^2 \sin^2 ak_y
\end{aligned}
\tag{4.30}
$$

with $\gamma_x = \hbar\Delta_x/a$, $\gamma_y = \hbar\Delta_y/a$ and $\beta = \hbar^2/2ma^2$.

The Hamiltonian must be solved self-consistently together with the equation for the pair potential. These read [44] (with derivatives discretized on the lattice)

$$
\begin{aligned}
\gamma_x(r) = {}& -ig \sum_{E_n > 0} \left(u_n(x + a, y) - u_n(x - a, y) \right) v_n^*(x, y) \\
& - u_n(x, y) \left(v_n^*(x + a, y) - v_n^*(x - a, y) \right), \\
\gamma_y(r) = {}& g \sum_{E_n > 0} \left(u_n(x, y + a) - u_n(x, y + a) \right) v_n^*(x, y) \\
& - u_n(x, y) \left(v_n^*(x, y + a) - v_n^*(x, y + a) \right).
\end{aligned}
\tag{4.31}
$$

Here u_n and v_n are the electron and hole component of the wave function, respectively, and assumed to be from the tight-binding model, i.e.

they are dimensionless and represent the probability amplitude per lattice point (x, y).

The coupling constant g must be chosen such that it gives the correct pair potential γ in the bulk. It can be calculated as

$$
\begin{aligned}
\frac{\gamma}{g} &= \frac{1}{\pi^2} \int_{-\pi}^{\pi} d(ak_x) \int_{-\pi}^{\pi} d(ak_y) \, \sin(ak_x) \, u(\boldsymbol{k}) v^*(\boldsymbol{k}) \\
&= \frac{-i}{\pi^2} \int_{-\pi}^{\pi} d(ak_x) \int_{-\pi}^{\pi} d(ak_y) \, \sin(ak_y) \, u(\boldsymbol{k}) v^*(\boldsymbol{k}),
\end{aligned} \tag{4.32}
$$

where $u(\boldsymbol{k})$ and $v(\boldsymbol{k})$ are the electron and hole coefficients of the plane wave solutions of the bulk lattice Hamiltonian with $E > 0$.

In the particular case of a system that is translationally invariant in x-direction, as is the case for an infinitely extended line defect, the gap equations can be written as:

$$
\gamma_x(\boldsymbol{r}) = \frac{4g}{N_x} \sum_{E_n > 0, k_x} u_n(k_x, y) v_n^*(k_x, y) \, \sin(ak_x)
$$

$$
\gamma_y(\boldsymbol{r}) = \frac{g}{N_x} \sum_{E_n > 0, k_x}
$$

$$
\left(\left(u_n(k_x, y+a) - u_n(k_x, y+a) \right) v_n^*(k_x, y) \right.
$$

$$
\left. - u_n(k_x, y) \left(v_n^*(k_x, y+a) - v_n^*(k_x, y+a) \right) \right), \tag{4.33}
$$

summing over N_x longitudinal momenta k_x, and solving the tight-binding problem for each k_x individually.

The self-consistent solution of the tight-binding Hamiltonian and the gap equation (4.33) is obtained in an iterative procedure. In the iteration, we neglect the influence of the vector potential arising from local currents [44] as those effects are expected to be minor for the examples considered in this work. Furthermore, we also avoid adjusting the chemical potential U_0 to obtain a fixed number of electrons in the system and instead use a large unit cell so that the bulk value of Δ is recovered away from the defect.

Appendix 4.C   Line defect in the continuum limit

We calculate the closing and reopening of the excitation gap upon introduction of a line defect in the Hamiltonian (4.1), which is the continuum
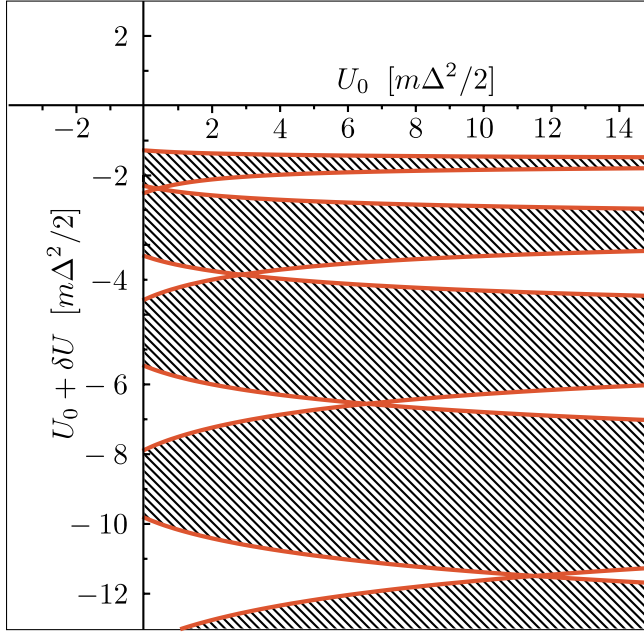
Figure 4.7. The red solid curves are the solution of Eq. (4.38) for $W = 4\hbar/m\Delta$. The MS states exist in the shaded regions.

limit ($a \to 0$) of the Wilson fermion lattice model of App. 4.A.1. The mode matching calculation presented here is the one-dimensional version of the two-dimensional calculation in Refs. [73, 72, 74].

The line defect, of width W, is formed by the electrostatic potential profile

$$U(\boldsymbol{r}) = \begin{cases} U_0 & \text{if } |y| > W/2, \\ U_0 + \delta U & \text{if } |y| < W/2. \end{cases} \qquad (4.34)$$

A zero-mode $\psi = (u, v)$ is a (doubly degenerate) eigenstate of the Hamiltonian (4.1) at $E = 0$, $p_x = 0$. The zero-mode should thus satisfy

$$(U + p_y^2/2m)u = i\Delta p_y v, \qquad (4.35a)$$

$$(U + p_y^2/2m)v = i\Delta p_y u. \qquad (4.35b)$$

For uniform U the solution is a plane wave,

$$\psi_{ss'} = e^{ik_{ss'}y}\begin{pmatrix} 1 \\ s \end{pmatrix}, \quad s, s' = \pm 1, \qquad (4.36)$$

with transverse wave vector

$$k_{ss'} = (m/\hbar)\left(is\Delta + s'\sqrt{-\Delta^2 - 2U/m}\right). \qquad (4.37)$$

In the region $|y| < W/2$ the zero-mode ψ is a superposition of the four states $\psi_{++}, \psi_{+-}, \psi_{-+}, \psi_{--}$. For $y > W/2$ two decaying states with $\mathrm{Im}\, k_{ss'} > 0$ appear in the superposition, while for $y < -W/2$ the other two states with $\mathrm{Im}\, k_{ss'} < 0$ appear. In total ψ has eight unknown coefficients, which we determine by demanding continuity of ψ and $d\psi/dy$ at $y = W/2$ and $y = -W/2$. The determinant of this set of equations should vanish, in order to have a nontrivial solution. There is only a zero-mode for $U_0 > 0$, $U_0 + \delta U < -m\Delta^2/2$, determined by

$$\tan qW = \frac{2qq_0}{q^2 - q_0^2}. \qquad (4.38)$$

We have defined

$$q = (m/\hbar)\sqrt{-\Delta^2 - (2/m)(U_0 + \delta U)}, \qquad (4.39)$$

$$q_0 = (m/\hbar)\sqrt{\Delta^2 + 2U_0/m}. \qquad (4.40)$$

The MS states exist in between subsequent gap closings, as indicated in Fig. 4.7 (shaded regions).